ACSNANO

www.acsnano.org

ARTICLE

Space-Confinment-Enhanced Fluorescence Detection of DNA on Hydrogel Particles Array

Fei Liu,[#] Yuemeng Yang,[#] Xizi Wan, Hongxiao Gao, Yulu Wang, Jingwei Lu, Li-Ping Xu,* and Shutao Wang

Cite This: *ACS Nano* 2022, 16, 6266−6273

Read Online

ACCESS | Metrics & More | Article Recommendations | Supporting Information

ABSTRACT: **Fluorescent biosensors have been widely applied in DNA detection because of their reliability and reproducibility. However, low kinetics in DNA hybridization often brings out long test terms, thus restricting their practical use. Here, we demonstrate unexpected fast DNA fluorescence detection on the confined surface of hydrogel particles. When the pore size and surface charge of hydrogel particles are tailored, DNA molecules can be confined in the outer water layer of hydrogel particles. We fabricated a fluorescence-on DNA sensor based on the hydrogel particle array by utilizing the fluorescence quenching property of graphene oxide and its different adsorption behaviors toward single-strand DNA or double-strand DNA. Benefiting from the confinement effect of hydrogel particle surface and the enrichment effect of water evaporation, the DNA-recognition time was descreased significantly from 3000 s to less than 10 s under the target concentration of 400 nM. Moreover, rapid detection can be achieved at concentrations between 50 and 400 nM. The study provides another insight to fabricate fast biosensors and shows great potential in DNA diagnostics, gene analysis, and liquid biopsy.**

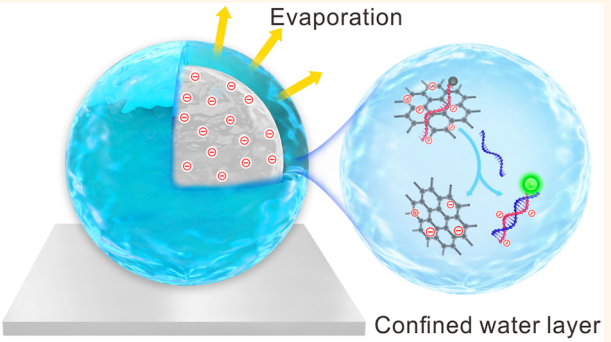

KEYWORDS: *space-confinement, hydrogel particle, fluorescent signal detection, fast DNA hybridization kinetics, biosensor*

The abnormal expression of some deoxyribonucleic acid (DNA) is associated with a variety of human diseases, highlighting its great potential as a valuable biomarker in the diagnostics, prognostics, and treatment of diseases.[1,2] In recent years, due to the high sensitivity and little sample damage, the fluorescent method has been developed as a reliable and reproducible approach for DNA detection.[3−6] Despite the excellent sensitivity of fluorescent biosensors, the fluorescent DNA biosensor still meets a challenge in detecting ultratrace samples. In a homogeneous bulk solution, the recognition between DNA capture probes and target DNA reactants relies on their random collision and interaction. For ultratrace DNA detection, the biosensing proceeding involves continuously searching for the target DNA in the solution. Due to the low mass transfer efficiency, the reaction time is prominently prolonged, with compromised recognition efficiency.[7] Therefore, it remains an intractable challenge to accelerate the slow reaction kinetics for ultratrace DNA detection.

Nature confines the interacting species into small volumes to alter the apparent interaction kinetics and promote molecular encountering. For example, by confining the receptor into nanosized domains on the cell surface, the T-cell can sense and distinguish specific peptides at ultralow concentration.[8−11] Compared with that of the conventional bulk aqueous solution, the localized concentration may be increased by several orders of magnitude, which generally leads to a drastic increase in the encounter rates and the binding affinity. This natural space-confinement mechanism has given inspiration for DNA biosensing and cell imaging.[12−14] The 2D or 3D DNA assemblies, such as DNA origami,[15,16] 3D DNA walker,[7,17−19] etc. were designed to confine the reactants or signal reporter in a compact space to increase local concentration, thereby accelerating the reaction and improving efficiency.[20,21] However, multiple hybridization steps and precise design in the DNA self-assembly strategy will significantly hinder their wide applications in biosensing.

Received: January 6, 2022
Accepted: April 4, 2022
Published: April 6, 2022

https://doi.org/10.1021/acsnano.2c00157
ACS Nano 2022, 16, 6266−6273

Scheme 1. Schematic Illustrations of Fluorescence DNA Detection Based on Space-Confinement Hydrogel Particles[a]

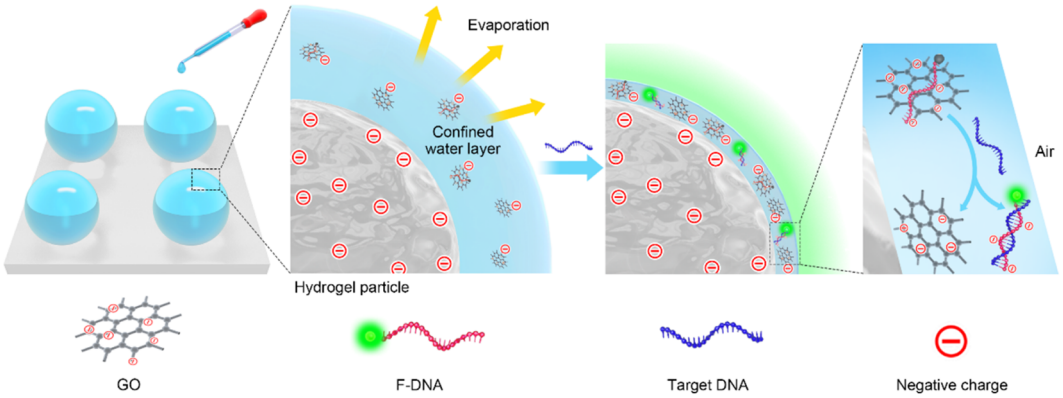

[a]The compact structure of the hydrogel surface and the repulsive force between negatively charged hydrogel and DNA nucleotide prevent the DNA molecules from entering the interior of hydrogel. The analyte solution can be confined in the outer water layer of hydrogel particles, thereby achieving the enrichment effect and accelerating the reaction process.

Herein, we developed a DNA biodetection platform with accelerated kinetics based on the confined outer water layer of hydrogel particles, and the reaction rate is 300-fold faster than that of the bulk solution. By careful optimization of the surface charge and pore size of hydrogel particles, the analyte solution can be confined in the outer water layer of the hydrogel particles (Scheme 1). With subsequent water evaporation, the analyte can be further enriched at the surface of the hydrogel particle. Graphene oxide (GO) can absorb single-stranded DNA and repel double-stranded DNA.[22−26] Based on the distinct adsorption behavior and the fluorescence quenching effect of GO, the DNA detection platform was established by using 6-carboxylfluorescein (FAM) labeled DNA (F-DNA) as a signal probe and GO as a background reducer. The biorecognition process at the confined water layer can be accelerated dramatically, allowing sensitive DNA detection. The generic hydrogel particle-based biosensing platform holds considerable promise for sensitive bioanalysis.

RESULTS AND DISCUSSION

Characterization of the PEG Hydrogel Particles Array. Superhydrophilic microwells array on the superhydrophobic surface was employed to fabricate the PEG hydrogel particles array (Figure S1). Benefiting from the wettability difference of the superhydrophilic microwell and superhydrophobic surface, the 2 μL hydrogel precursor solution can be steadily anchored on the superhydrophilic microwell, forming a regular PEG hydrogel array without cross-contamination after UV polymerization, as shown in Figure 1a and Figure S2. The hydrogel particle's water contact angle (WCA) is 0°, which reveals the hydrogel's hydrophilicity (Figure 1b,i).[27] The substrate demonstrates extreme water repellency with a contact angle of 154.7 ± 2.1° due to the modification of 1*H*,1*H*,2*H*,2*H*-perfluorodecyltrichlorosilane (FDTS) with low surface energy (Figure 1b,ii). The microstructure of the freeze-dried hydrogel was observed by a scanning electron microscope (SEM). The cross-linking density of the hydrogel is a significant factor that affects the pore size of the hydrogel network, which is dependent on the molecular weight (MW) of PEG-DA.[28] We use pure PEG-DA (MW700) to generate a small porous microstructure. SEM characterization of the hydrogels (Figure 1c,d) demonstrates that dense structure was formed on the surface and the external of the hydrogel, which is consistent with literature reports.[28,29] As shown in Figure S3, the hydrogel contains infrared characteristic peaks of PEG-DA, PEG, and acryl-PEG-COOH.

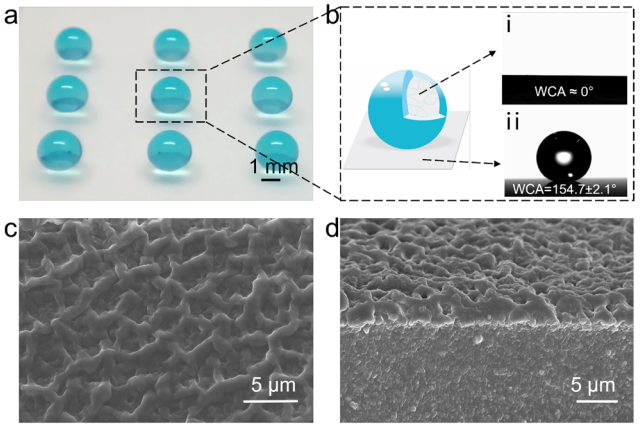

Figure 1. Characterization of the PEG hydrogel particles array. (a) Photograph of PEG hydrogel particles array, dyed with methylene blue trihydrate (MBT). (b) Water contact angles (WCA) of PEG hydrogel particles (i) and superhydrophobic substrate (ii). (c) Top-view SEM image of the PEG hydrogel particles. (d) Cross-sectional view SEM image of the PEG hydrogel particles.

Distribution of DNA Molecules on the Hydrogel Particles. The influence of the hydrogel charge on the DNA molecules distribution was investigated. We have synthesized three different hydrogel particles, namely, PEG-COOH-1 hydrogel particles, PEG hydrogel particles, and MAETAC-PEGDA hydrogel particles. ζ potential measurements confirm that the above three kinds of hydrogel particles are negatively charged, neutrally charged, and positively charged, respectively (Figure 2a−c, Figure S4). Furthermore, SEM image demonstrates that dense structure was also formed on all those three kinds of hydrogel paricles (Figure S5). The distribution results of DNA on hydrogel particles were characterized by laser scanning confocal microscope (LSCM). (See the Instruments and Characterization section.)

For negatively charged PEG-COOH-1 hydrogel particles, F-DNA molecules are mainly distributed in the outer water layer of the hydrogel particles (Figure S7a). The continuous evaporation of the outer water layer can enrich the F-DNA,

https://doi.org/10.1021/acsnano.2c00157
ACS Nano 2022, 16, 6266−6273

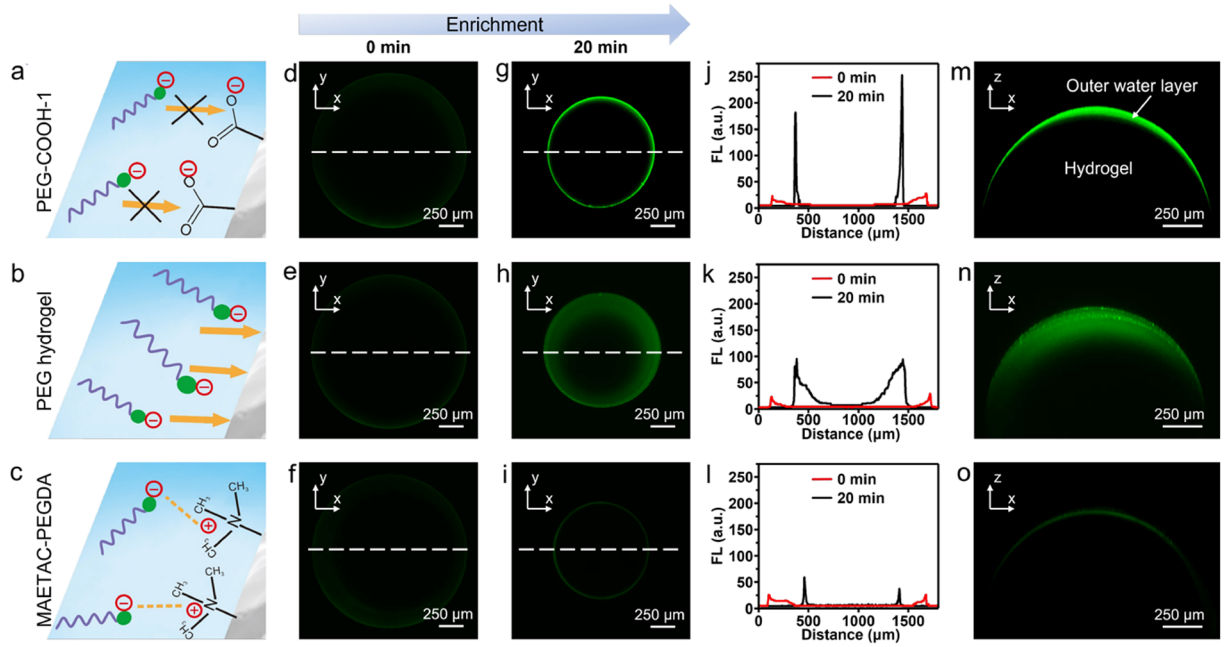

Figure 2. Distribution of DNA molecules on hydrogel particles with different charges. (a)−(c) Schematics of the interaction between hydrogel particles and F-DNA molecules. Fluorescence images of F-DNA droplets on different hydrogel particles after evaporation for 0 min (d)−(f) and 20 min (g)−(i) at room temperature and 25% relative humidity. (j)−(l) Corresponding cross-section analysis of F-DNA droplets on hydrogel particles. (m)−(o) Sideview LSCM tomography images of F-DNA droplets on different hydrogel particles after evaporating for 20 min. Fluorescence images were obtained by the LSCM, and the excitation light source is 488 nm.

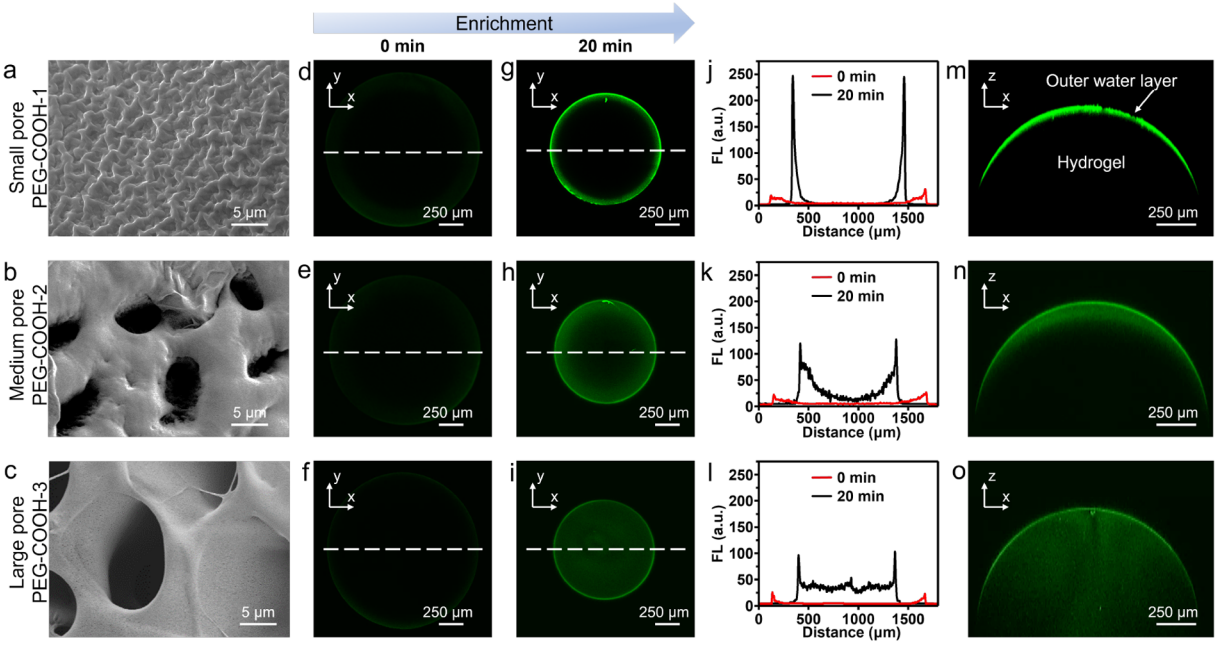

Figure 3. Distribution of DNA molecules on hydrogel particles with different pore sizes. SEM images of dried hydrogel particles with different pore sizes: (a) small pore size (PEG-COOH-1) (average pore size, 0.95 ± 0.22 μm), (b) medium pore size (PEG-COOH-2) (average pore size, 4.28 ± 1.02 μm), and (c) large pore size (PEG-COOH-3) (average pore size, 8.72 ± 1.58 μm). Fluorescence images of F-DNA droplets on different hydrogel particles after evaporation for 0 min (d)−(f) and 20 min (g)−(i) at room temperature and 25% relative humidity. (j)−(l) Corresponding cross-section analysis of F-DNA droplets on hydrogel particles. (m)−(o) Sideview LSCM tomography images of F-DNA droplets on different hydrogel particles after evaporating for 20 min. Fluorescence images were obtained by the LSCM, and the excitation light source is 488 nm.

which results in the increase of fluorescence intensity with time (Figure 2d, g, j). LSCM tomography images and 3D fluorescence images (Figure 2m, Figure S8a) further proved that F-DNA molecules were confined in the outer water layer of the hydrogel particles, which may be caused by the electrostatic repulsion between the hydrogel particle and the F-DNA. In contrast, for the neutral PEG hydrogel particles, the fluorescent DNA molecules can gradually diffuse inside of the

https://doi.org/10.1021/acsnano.2c00157
ACS Nano 2022, 16, 6266−6273

hydrogel (Figure S7a). After evaporation, an obvious fluorescent signal appeared inside the hydrogel particles (Figure 2e, h, k). LSCM tomography images and 3D fluorescence images (Figure 2n, Figure S8b) show that the F-DNA molecules are distributed inside the hydrogel particles. For the positively charged MAETAC-PEGDA hydrogel particles, fluorescence images showed the irregular distribution of fluorescence signal on the MAETAC-PEGDA hydrogel particles after 20 min of evaporation (Figure 2f, i, o). The cross-section analysis also showed low fluorescence values both inside and on the surface of the hydrogel (Figure 2l). This may be due to the aggregation-caused quenching of F-DNA on the hydrogel surface. Due to electrostatic attraction force, DNA can be rapidly adsorbed on the surface (Figure S7a), resulting in quenching of the fluorescence signal. The above results indicate that only the negatively charged hydrogel particles can confine DNA molecules in the outer water layer. This confinement effect may favor the biorecognition process in biosensing.

The pore size effect of the hydrogel particles on the distribution of DNA molecules was further investigated. The pore size of the hydrogel particles can be tuned by optimizing the molecular weight of PEG-DA. The smaller the molecular weight is, the denser the hydrogel structure is.[28] SEM images confirm that three different hydrogels with different pore sizes were fabricated (Figure 3a–c, Figure S6).

The compact structure of the PEG-COOH-1 hydrogel surface prevents the F-DNA molecules from entering the interior of the hydrogel (Figure S7b). The F-DNA molecules were enriched from the diluted solution on the surface of the PEG-COOH-1 hydrogel particle, which can achieve the amplification of fluorescent signals (Figure 3d, g, j). As for PEG-COOH-2 hydrogel particles with pore sizes of about 4.28 μm, some F-DNA molecules entered the interior of hydrogel (Figure 3e, h, k). Further increasing the pore size to 8.72 μm (PEG-COOH-3) leads to more F-DNA molecules entering the hydrogel inside (Figure 3f, i, o). LSCM tomography images and 3D fluorescence images further confirmed that the smallest pore size of the hydrogel has the best confinement effect (Figure 3m–o, Figure S8d–f). However, the fluorescent bright rings due to the space-confined effect of F-DNA can be observed on all negatively charged hydrogel surface, regardless of the pore size of the negatively hydrogel (Figure 3j–l), which indicated that electrostatic repulsion prevents DNA from entering hydrogel interior by diffusion. Therefore, it has been established that the charge property of particle surface is the dominant factor for space-confinement. In addition, the control of pore size is also crucial for DNA space-confinement. The best confinement effect can be obtained through the synergy of pore size and charge.

Moreover, the effect of evaporation time and humidity on the output signal were optimized (Figure S9). Considering the efficiency of detection and space-confinement effect, 25% humidity and 20 min evaporation time were used as the optimal conditions.

On the basis of the above discussion, the negatively charged hydrogel with small-pore size (PEG-COOH-1) has the best confinement effect, enriching DNA molecules on the surface of the hydrogel particles. Hence, PEG-COOH-1 hydrogel particles were used to fabricate hydrogel particle-based DNA sensors (HP-based DNA sensors).

Optimization of HP-Based DNA Sensor. The PEG-COOH-1 hydrogel particle is used to fabricate confined space for DNA detecting. GO can quench the fluorescence of F-DNA via remotely fluorescence resonance energy transfer (FRET).[23] As shown in Figure S1, with the presence of target DNA, the fluorescence can be recovered due to the formation of F-DNA/target DNA duplex structure.[33] All the ssDNA sequences used in our work are listed in Table S1 (see the Supporting Information).

Interaction between different DNA strands was validated by analyzing agarose gel electrophoresis experiments (Figure S10). Furthermore, as shown in Figure S11, the GO can be confined in the outer water layer of the hydrogel particles throughout the experiment (within 40 min). The concentration of GO and quenching time of F-DNA were optimized. The fluorescence intensity of F-DNA on the hydrogel decreases along with increasing the concentration of GO and reaches a plateau at 80 μg/mL GO, as shown in Figure 4a.

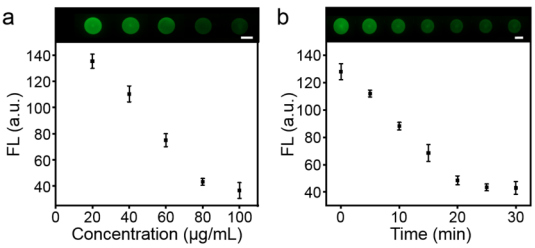

Figure 4. Optimization of DNA detecting conditions on the surface of the hydrogel particle. (a) Fluorescence response of F-DNA in the presence of GO with different concentrations. The concentration of F-DNA is 100 nM. Scale bar: 1 mm. (b) Real-time fluorescence image and corresponding intensity of the quenching reaction between F-DNA and GO. The insets are the corresponding fluorescence images. Scale bar: 1 mm. The fluorescence images were obtained by the biological fluorescence microscope, and the excitation light source is 488 nm.

Therefore, 80 μg/mL of GO was selected for the following experiments. Figure 4b shows that the fluorescence intensity of F-DNA gradually decreases first due to the quenching effect of GO and then reaches the plateau at 20 min. Hence, 80 μg/mL of GO concentration and 20 min quenching time were used for DNA detection.

Performance of HP-Based DNA Sensor. The fabricated DNA biosensor based on PEG-COOH-1 hydrogel particle was employed for DNA detection. Under the optimal conditions, the analytical performance was evaluated at different concentrations of DNA. As can be seen from Figure S12, the maximum signal response was obtained at the concentration of 400 nM. Surprisingly, after adding 400 nM target DNA, the fluorescence of FAM intensity is recovered quickly and reaches the plateau within 10 s (Figure 5a). Fast DNA hybridization kinetics using the hydrogel particle-based space-confinement platform was observed. For comparison, the DNA detection in conventional bulk aqueous solution demonstrated relatively slow DNA hybridization kinetics. The maximum signal was obtained within 3000 s, which is 300-fold slower than in the space-confinement HP-based DNA sensor.

The DNA hybridization reaction is an interchain reaction of macromolecules, which can be regarded as an association reaction involving diffusion in three-dimensional finite domains.[34] The hybridization reaction of two complementary ssDNA might be symbolized as the following:[35,36]

https://doi.org/10.1021/acsnano.2c00157
ACS Nano 2022, 16, 6266–6273

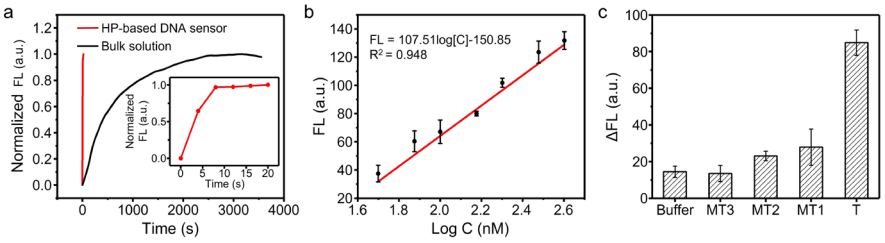

Figure 5. Performance of HP-based DNA sensor. (a) Real-time fluorescence intensities of adding 400 nM target DNA on the HP-based DNA sensor and the bulk solution. The inset is the enlarged view of real-time fluorescence intensities based on the HP-based DNA sensor. (b) Fluorescence intensity response after adding target DNA with different concentrations. (c) Fluorescent intensity response of HP-based DNA sensor after adding buffer solution (buffer), 400 nM target DNA (T), 400 nM single-base mismatch DNA (MT1), 400 nM two-base mismatch DNA (MT2), and 400 nM three-base mismatch DNA (MT3). The error bars are the standard deviation from three independent experiments.

$$SS_1 + SS_2 \underset{k_{off}}{\overset{k_{on}}{\rightleftharpoons}} SS_1{\cdot}SS_2 \xrightarrow{k_r} \text{duplex (P)} \quad (1)$$

where SS_1 and SS_2 refer to the two complementary single strands, k_{on} and k_{off} represent the formation and dissociation rates constant of $SS_1{\cdot}SS_2$, respectively, k_r is the formation rates constant of double-stranded DNA (P), using the following rate equation:

$$r = \frac{d[\text{duplex}]}{dt} = k_{on}[SS_1][SS_2] - k_{off}[SS_1{\cdot}SS_2] - k_r[SS_1{\cdot}SS_2] \quad (2)$$

Nucleation and diffusion are two main kinetic limiting steps in DNA hybridization. The nucleation step means taking single-stranded DNA to a nucleated duplex with two to four H-bonded and stacked bases ($SS_1{\cdot}SS_2$), and this nucleation step is followed by a rapid zipping step in which the rest of the duplex base stacks and hydrogen bonds.[37]

Equation 2 can be simplified as

$$r = k_{on}[SS_1][SS_2] \quad (3)$$

According to the diffusion model and Fick's first law, when the distance between SS_1 and SS_2 is L, the flux of SS_2 is

$$J = -D_{SS_2}\frac{dN_{SS_2}}{dL} \quad (4)$$

where J is the flux of the diffusing particles SS_2, D_{SS_2} is the diffusion coefficient, and $\frac{dN_{SS_2}}{dL}$ is the concentration gradient of the SS_2.

According to eqs 3 and 4, the total rate r of hybridization reaction in a unit volume for eq 1 is

$$r = 4\pi(D_{SS_1} + D_{SS_2})L_{SS_1{\cdot}SS_2}N^0_{SS_1}N^0_{SS_2} \quad (5)$$

In that expression, D_{SS_1} and D_{SS_2} refer to the diffusion coefficient and $N^0_{SS_1}$ and $N^0_{SS_2}$ are the bulk concentrations of SS_1 and SS_2. $L_{SS_1{\cdot}SS_2}$ is the distance between SS_1 and SS_2. In the HP-based DNA sensor, the DNA molecules are enriched in the outer water layer of the hydrogel particles. The bulk concentration of SS_1 ($N^0_{SS_1}$) increases significantly due to the evaporation effect,[38] which leads to the higher hybridization kinetics. Furthermore, another possible reason is that the conformation of ssDNA is stretched in the confined space. F-DNA is enriched in a gradually concentrated confined environment, and electrostatic repulsion between DNA and hydrogel provides a stretching force, altering the conformation of the ssDNA from random coil to stretched conformation. Thus, the intramolecular secondary structure in randomly coiled structure was eliminated, which might promote DNA hybridization and speed up the reaction rate.[39−41]

The performance of the HP-based DNA sensor was investigated. Fluorescence intensity gradually increased with the increasing of the concentration of target DNA; as shown in Figure 5b, the fluorescence intensity increased linearly with the logarithm of target DNA concentration from 50 to 400 nM with a calibration function of FL = 107.51 log C − 150.85 (correlation coefficient of 0.948, FL is the fluorescence intensity, and C is the concentration of target DNA). The limit of detection of the biosensor was calculated to be down to 26.3 nM (based on the blank signal plus 3 times the standard deviation of the blank signal). The specificity of the sensor was also studied by comparing the fluorescence response of the target DNA to the background signal (Buffer), single-base mismatch target (MT1), the two-base mismatch target (MT2), and the three-base mismatch target (MT3), respectively. As shown in Figure 5c, compared with the fluorescence of the target DNA (T), the fluorescence response of MT1, MT2, and MT3 at the same concentration is almost at the same level of the background signals. These results show that the sensor has reasonable specificity for detecting target DNA. As shown in Figure S13, detection of target DNA in serum was achieved by the space-confinement biosensor. The results obtained in 1% serum were consistent with those obtained in Tris−HCl buffer, which implies this biosensor shows great anti-interference ability and can be used for DNA detection in serum samples.

The developed assay was further compared with other fluorescent biosensors (Table S2). As shown in Table S2, this simple method can improve the detection speed of DNA by more than 100 times. The limit of detection (LOD) can be further reduced by introducing various amplification systems, which will be studied in our following work. In short, these above experiment results indicated that the as-proposed HP-based DNA sensor have a great advantage with other fluorescent biosensors on detection time, exhibiting great potential as a reliable platform for rapid detection of DNA.

CONCLUSIONS

In summary, we have developed a space-confinement strategy based on hydrogel particles toward DNA detection with significant fast hybridization kinetics (within 10 s at 400 nM target DNA). The fabricated hydrogel particles can confine the

https://doi.org/10.1021/acsnano.2c00157
ACS Nano 2022, 16, 6266−6273

DNA molecules in the outer water layer through the synergy of pore size and charge. The water evaporation leads to the further enrichment of detection probes and targets. The confinement effect of the hydrogel particles improved the DNA hybridization efficiency by 300 times compared with that of the solution. The developed hydrogel particle-based DNA sensor is simple to fabricate and can be extended to assay proteins, exosomes, cells, etc. We expect this work to have broad application in clinic liquid biopsy and personalized medicine.

METHODS

Fabrication of Superwettable Microchips. Acid-catalyzed silica sol (ACSS) was synthesized according to ref 42. A 6.5 g sample of TEOS was dissolved in 53.25 g of ethanol, and the solution was mixed with 0.0125 g of concentrated HCl solution. The solution was left in a closed flask, stirred for 4 h, and aged for 4 days at room temperature. Two grams of SiO_2 was dispersed in 80 mL of ethanol and stirred for 2 h. Then 20 μL of ACSS was added to the mixture solution, stirring for an additional 1 h to obtain the SiO_2 suspension for further use.

The glass (38 mm × 23 mm) was cleaned by sonication in acetone, ethanol, and deionized water sequentially and then dried with nitrogen.[43] After plasma treatment, the glass was repeatedly dipcoated with the above SiO_2 suspension coatings 10 times. Then, in order to obtain superhydrophobic substrate, the glass was immersed into the FDTS solution (FDTS: anhydrous toluene = 1:1000) for 30 min at room temperature, followed by rinsing with pure ethanol and heating solidification at 80 °C for 20 min.[44]

The FDTS-modified superhydrophobic substrate was treated by oxygen plasma through a photomask for 30 s to form superwettable microchips (Figure S1).

Fabrication of Hydrogel Particles Array. *Fabrication of the PEG-COOH-1 Hydrogel Particles.* Two microliters of precursor solution containing 40% (v/v) PEG (MW 200), 20% (v/v) PEG-DA (MW 700), 10% (v/v) acryl-PEG-COOH aqueous solution (20 mM, MW 3400), and 10% (v/v) 2-hydroxy-2-methylpropiophenone (photoinitiator) ethanol solution (655 mM) was added into the superhydrophilic point. The whole system was irradiated by 365 nm UV (60 mW/cm^2) for 10 s to form the PEG hydrogel particle array. The prepared hydrogel array was kept in DI water or a highly humid environment until use.[29]

PEG-DA (MW700) and PEG-DA (MW3400) were selected as cross-linking agents, the ratio of which was adjusted to obtain hydrogel particles with different pore sizes (PEG-COOH-2 and PEG-COOH-3) under the same polymerization conditions.

Fabrication of the PEG-COOH-2 Hydrogel Particles. The 40% (v/v) PEG (MW 200), 15% (v/v) PEG-DA (MW 3400, 20 mM) aqueous solution, 15% (v/v) PEG-DA (MW 700), 15% (v/v) acryl-PEG-COOH aqueous solution (20 mM), and 10% (v/v) 2-hydroxy-2-methylpropiophenone (photoinitiator, 655 mM) ethanol solution were mixed in DI water.

Fabrication of the PEG-COOH-3 Hydrogel Particles. The 7.5% (v/v) PEG-DA (MW 700), 22.5% (v/v) PEG-DA (MW 3400, 20 mM) aqueous solution, 40% (v/v) PEG (MW 200), 15% (v/v) acryl-PEG-COOH aqueous solution (20 mM), and 10% (v/v) 2-hydroxy-2-methylpropiophenone (photoinitiator, 655 mM) ethanol solution were mixed in DI water.

PEG and MAETAC-PEGDA were selected to fabricate neutrally and positively charged hydrogel particles, respectively.

Fabrication of the PEG Hydrogel Particles. The 40% (v/v) PEG (MW 200), 20% (v/v) PEG-DA (MW 700), and 10% (v/v) 2-hydroxy-2-methylpropiophenone (photoinitiator) ethanol solution (655 mM) were mixed in DI water.

Fabrication of the MAETAC-PEGDA Hydrogel Particles.[30−32] The MAETAC-PEGDA hydrogel particles were made by dissolving PEG-DA (MW700) into 20 mM HEPES buffer saline (pH = 7.4) containing 10% (v/v) of 2-hydroxy-2-methylpropiophenone ethanol solution (655 mM) as the photoinitiator to get a final concentration of 17%. The positively charged hydrogels were produced by adding MAETAC at 200 mM into the PEG-DA solution.

Fluorescence Detection of DNA on Hydrogel Particles Array. The oligonucleotides were diluted with Tris−HCl buffer (20 mM Tris−HCl, 50 mM KCl, 10 mM $MgCl_2$). The dissolved DNA solution was first heated for 5 min at 95 °C and then gradually cooled to room temperature before use. Two microliters of the precursor mixture (80 μg/mL GO, 100 nM F-DNA) was added to the hydrogel particles at room temperature, and the resulting mixture was mixed for 20 min on an HP-based DNA sensor platform. Two microliters of the target probe of different concentrations was then added to the platform, and the fluorescence intensity of the system was measured.

Fluorescence Detection of DNA in Human Serum. The human serum was diluted to 1% with Tris−HCl buffer (20 mM Tris−HCl, 50 mM KCl, 10 mM $MgCl_2$). The preparation of the HP-based DNA sensor platform was the same as before. The target DNA (diluted with 1% human serum) was then added and the fluorescence intensity was recorded.

ASSOCIATED CONTENT

Supporting Information

The Supporting Information is available free of charge at https://pubs.acs.org/doi/10.1021/acsnano.2c00157.

Materials and reagents, instruments and characterization details, tables of DNA oligonucleotide sequences and comparision with other fluorescent biosensors without amplification reaction, figures of hydrogel particle arrays and space-confinement sensors fabrication, characterization of the hydrogel stability, FTIR spectra, ζ potential values, SEM images, distribution and arrangement of DNA molecules, agarose gel electrophoresis, fluorescence images, detection of target DNA in the Tris−HCl buffer and serum (PDF)

Rinsing the hydrogel particle-based substrate with water (MP4)

AUTHOR INFORMATION

Corresponding Author

Li-Ping Xu − *Beijing Key Laboratory for Bioengineering and Sensing Technology, School of Chemistry and Biological Engineering, University of Science and Technology Beijing, Beijing 100083, China;* orcid.org/0000-0002-2683-7963; Email: xuliping@ustb.edu.cn

Authors

Fei Liu − *Beijing Key Laboratory for Bioengineering and Sensing Technology, School of Chemistry and Biological Engineering, University of Science and Technology Beijing, Beijing 100083, China*

Yuemeng Yang − *Beijing Key Laboratory for Bioengineering and Sensing Technology, School of Chemistry and Biological Engineering, University of Science and Technology Beijing, Beijing 100083, China*

Xizi Wan − *CAS Key Laboratory of Bio-inspired Materials and Interfacial Science, Technical Institute of Physics and Chemistry, Chinese Academy of Sciences, Beijing 100190, China*

Hongxiao Gao − *Beijing Key Laboratory for Bioengineering and Sensing Technology, School of Chemistry and Biological Engineering, University of Science and Technology Beijing, Beijing 100083, China*

Yulu Wang − *Beijing Key Laboratory for Bioengineering and Sensing Technology, School of Chemistry and Biological*

https://doi.org/10.1021/acsnano.2c00157
ACS Nano 2022, 16, 6266−6273

Engineering, University of Science and Technology Beijing, Beijing 100083, China

Jingwei Lu − *Beijing Key Laboratory for Bioengineering and Sensing Technology, School of Chemistry and Biological Engineering, University of Science and Technology Beijing, Beijing 100083, China*

Shutao Wang − *CAS Key Laboratory of Bio-inspired Materials and Interfacial Science, Technical Institute of Physics and Chemistry, Chinese Academy of Sciences, Beijing 100190, China; University of Chinese Academy of Sciences, Beijing 100049, China;* orcid.org/0000-0002-2559-5181

Complete contact information is available at: https://pubs.acs.org/10.1021/acsnano.2c00157

Author Contributions

#F.L. and Y.Y. contributed equally to this work.

Author Contributions

The manuscript was written through contributions of all authors. All authors have given approval to the final version of the manuscript.

Notes

The authors declare no competing financial interest.

ACKNOWLEDGMENTS

The work is supported by National Natural Science Foundation of China (21890742), National Key R&D Program of China (2019YFA0709300), Beijing Municipal Science and Technology Commission (2182036).

REFERENCES

(1) Sassolas, A.; Leca-Bouvier, B. D.; Blum, L. J. DNA Biosensors and Microarrays. *Chem. Rev.* **2008**, *108*, 109−139.

(2) Ma, F.; Ren, M.; Zhang, C.-y. Advances in single-particle detection for DNA sensing. *Sci. China Chem.* **2017**, *60*, 1285−1292.

(3) Li, C.; Li, H.; Ge, J.; Jie, G. Versatile fluorescence detection of microRNA based on novel DNA hydrogel-amplified signal probes coupled with DNA walker amplification. *Chem. Commun. (Camb.)* **2019**, *55*, 3919−3922.

(4) Wang, J.; Aki, M.; Onoshima, D.; Arinaga, K.; Kaji, N.; Tokeshi, M.; Fujita, S.; Yokoyama, N.; Baba, Y. Microfluidic biosensor for the detection of DNA by fluorescence enhancement and the following streptavidin detection by fluorescence quenching. *Biosens. Bioelectron.* **2014**, *51*, 280−285.

(5) Chen, Y.; Li, K.; Zhang, S.; Qin, L.; Deng, S.; Ge, L.; Xu, L. P.; Ma, L.; Wang, S.; Zhang, X. Bioinspired Superwettable Microspine Chips with Directional Droplet Transportation for Biosensing. *ACS Nano* **2020**, *14*, 4654−4661.

(6) Xu, T.; Xu, L. P.; Zhang, X.; Wang, S. Bioinspired superwettable micropatterns for biosensing. *Chem. Soc. Rev.* **2019**, *48*, 3153−3165.

(7) Chai, H.; Miao, P. Bipedal DNA Walker Based Electrochemical Genosensing Strategy. *Anal. Chem.* **2019**, *91*, 4953−4957.

(8) Ellis, R. J. Macromolecular crowding: obvious but underappreciated. *Trends Biochem. Sci.* **2001**, *26*, 597−604.

(9) Tan, Z. J.; Chen, S. J. Ion-mediated RNA structural collapse: effect of spatial confinement. *Biophys. J.* **2012**, *103*, 827−836.

(10) Tabaka, M.; Kalwarczyk, T.; Holyst, R. Quantitative influence of macromolecular crowding on gene regulation kinetics. *Nucleic Acids Res.* **2014**, *42*, 727−738.

(11) Nakano, S.; Miyoshi, D.; Sugimoto, N. Effects of molecular crowding on the structures, interactions, and functions of nucleic acids. *Chem. Rev.* **2014**, *114*, 2733−2758.

(12) Gooding, J. J.; Gaus, K. Single-Molecule Sensors: Challenges and Opportunities for Quantitative Analysis. *Angew. Chem., Int. Ed. Engl.* **2016**, *55*, 11354−11366.

(13) Shin, S.; Kim, H. S.; Kim, M. I.; Lee, J.; Park, H. G.; Kim, J. Crowding and confinement effects on enzyme stability in mesoporous silicas. *Int. J. Biol. Macromol.* **2020**, *144*, 118−126.

(14) Bui, H.; Miao, V.; Garg, S.; Mokhtar, R.; Song, T.; Reif, J. Design and Analysis of Localized DNA Hybridization Chain Reactions. *Small* **2017**, *13*, 1602983.

(15) Wang, D.; Fu, Y.; Yan, J.; Zhao, B.; Dai, B.; Chao, J.; Liu, H.; He, D.; Zhang, Y.; Fan, C.; Song, S. Molecular logic gates on DNA origami nanostructures for microRNA diagnostics. *Anal. Chem.* **2014**, *86*, 1932−1936.

(16) Bui, H.; Shah, S.; Mokhtar, R.; Song, T.; Garg, S.; Reif, J. Localized DNA Hybridization Chain Reactions on DNA Origami. *ACS Nano* **2018**, *12*, 1146−1155.

(17) Pang, H.; Xu, X.; Jiang, W. A track-regenerated DNA walker: Construction and its derived sensing application. *Sens. Actuators B Chem.* **2020**, *314*, 128053.

(18) Oishi, M.; Saito, K. Simple Single-Legged DNA Walkers at Diffusion-Limited Nanointerfaces of Gold Nanoparticles Driven by a DNA Circuit Mechanism. *ACS Nano* **2020**, *14*, 3477−3489.

(19) Yang, X.; Tang, Y.; Mason, S. D.; Chen, J.; Li, F. Enzyme-Powered Three-Dimensional DNA Nanomachine for DNA Walking, Payload Release, and Biosensing. *ACS Nano* **2016**, *10*, 2324−2330.

(20) Yang, F.; Cheng, Y.; Cao, Y.; Zhang, Y.; Dong, H.; Lu, H.; Zhang, X. MicroRNA Triggered DNA "Nano Wheel" for Visualizing Intracellular microRNA via Localized DNA Cascade Reaction. *Anal. Chem.* **2019**, *91*, 9828−9835.

(21) Li, X.; Liu, L.; Yin, F.; Liu, Y.; Xu, S.; Jiang, W.; Wang, R.; Xue, Q. In situ generation spatial confinement fluorescence RNA for sensitive and stable imaging of telomerase RNA in cells. *Sens. Actuators B Chem.* **2021**, *345*, 130414.

(22) Zhang, S.; Shi, W.; Li, K.-B.; Chen, F.; Su, J.; Han, D.-M. Graphene oxide/silver nanoclusters based logic devices and their application to multiplexed analysis of miRNA. *Sens. Actuators B Chem.* **2018**, *273*, 408−417.

(23) Zhou, C.; Liu, D.; Wu, C.; Liu, Y.; Wang, E. Integration of DNA and graphene oxide for the construction of various advanced logic circuits. *Nanoscale* **2016**, *8*, 17524−17531.

(24) Ghosh, T.; Mondal, A.; Vamsi Bharadwaj, S. V.; Mishra, S. A naturally fluorescent protein C-phycoerythrin and graphene oxide biocomposite as a selective fluorescence 'turn off/on' probe for DNA quantification and characterization. *Int. J. Biol. Macromol.* **2021**, *185*, 644−653.

(25) Shin, B.; Kim, W.-K.; Yoon, S.; Lee, J. Duplex DNA-functionalized graphene oxide: A versatile platform for miRNA sensing. *Sens. Actuators B Chem.* **2020**, *305*, 127471.

(26) Liu, X.; Aizen, R.; Freeman, R.; Yehezkeli, O.; Willner, I. Multiplexed Aptasensors and Amplified DNA Sensors Using Functionalized Graphene Oxide: Application for Logic Gate Operations. *ACS Nano* **2012**, *6*, 3553−3563.

(27) Song, Y.; Xu, T.; Xu, L. P.; Zhang, X. Nanodendritic gold/graphene-based biosensor for tri-mode miRNA sensing. *Chem. Commun. (Camb.)* **2019**, *55*, 1742−1745.

(28) Zhang, H.; Wang, L.; Song, L.; Niu, G.; Cao, H.; Wang, G.; Yang, H.; Zhu, S. Controllable properties and microstructure of hydrogels based on crosslinked poly (ethylene glycol) diacrylates with different molecular weights. *J. Appl. Polym. Sci.* **2011**, *121*, 531−540.

(29) Wu, L.; Wang, Y.; He, R.; Zhang, Y.; He, Y.; Wang, C.; Lu, Z.; Liu, Y.; Ju, H. Fluorescence hydrogel array based on interfacial cation exchange amplification for highly sensitive microRNA detection. *Anal. Chim. Acta* **2019**, *1080*, 206−214.

(30) Tan, F.; Xu, X.; Deng, T.; Yin, M.; Zhang, X.; Wang, J. Fabrication of positively charged poly (ethylene glycol)-diacrylate hydrogel as a bone tissue engineering scaffold. *Biomed. Mater.* **2012**, *7*, 055009.

(31) Dadsetan, M.; Knight, A. M.; Lu, L.; Windebank, A. J.; Yaszemski, M. J. Stimulation of neurite outgrowth using positively charged hydrogels. *Biomaterials* **2009**, *30*, 3874−3881.

(32) Wittmer, C. R.; Phelps, J. A.; Saltzman, W. M.; Van Tassel, P. R. Fibronectin terminated multilayer films: protein adsorption and cell attachment studies. *Biomaterials* **2007**, *28*, 851−860.
(33) Zhou, C.; Wang, K.; Fan, D.; Wu, C.; Liu, D.; Liu, Y.; Wang, E. An enzyme-free and DNA-based Feynman gate for logically reversible operation. *Chem. Commun. (Camb.)* **2015**, *51*, 10284−10286.
(34) Szabo, A.; Schulten, K.; Schulten, Z. First passage time approach to diffusion controlled reactions. *J. Chern. Phys.* **1980**, *72*, 4350−4357.
(35) Downs, A. M.; McCallum, C.; Pennathur, S. Confinement effects on DNA hybridization in electrokinetic micro-and nanofluidic systems. *Electrophoresis* **2019**, *40*, 792−798.
(36) Yamashita, K.; Miyazaki, M.; Yamaguchi, Y.; Nakamura, H.; Maeda, H. The change of activation energy in microchannel laminar flow as demonstrated by kinetic analysis of the DNA duplex-coil equilibrium. *Lab Chip* **2008**, *8*, 1171−1177.
(37) Wong, K. L.; Liu, J. Factors and methods to modulate DNA hybridization kinetics. *Biotechnol. J.* **2021**, *16*, 2000338.
(38) Xu, L. P.; Chen, Y.; Yang, G.; Shi, W.; Dai, B.; Li, G.; Cao, Y.; Wen, Y.; Zhang, X.; Wang, S. Ultratrace DNA Detection Based on the Condensing-Enrichment Effect of Superwettable Microchips. *Adv. Mater.* **2015**, *27*, 6878−6884.
(39) Gao, Y.; Wolf, L. K.; Georgiadis, R. M. Secondary structure effects on DNA hybridization kinetics: a solution versus surface comparison. *Nucleic Acids Res.* **2006**, *34*, 3370−3377.
(40) Li, F.; Mao, X.; Li, F.; Li, M.; Shen, J.; Ge, Z.; Fan, C.; Zuo, X. Ultrafast DNA Sensors with DNA Framework-Bridged Hybridization Reactions. *J. Am. Chem. Soc.* **2020**, *142*, 9975−9981.
(41) Hsieh, S. F.; Wei, H. H. Entropic trap, surface-mediated combing, and assembly of DNA molecules within submicrometer interfacial confinement. *Phys. Rev. E: Stat., Nonlinear, Soft Matter Phys.* **2009**, *79*, 021901.
(42) Du, X.; Xing, Y.; Zhou, M.; Li, X.; Huang, H.; Meng, X.-M.; Wen, Y.; Zhang, X. Broadband antireflective superhydrophilic antifogging nano-coatings based on three-layer system. *Microporous Mesoporous Mater.* **2018**, *255*, 84−93.
(43) Liu, Y.; Liu, Y.; Matharu, Z.; Rahimian, A.; Revzin, A. Detecting multiple cell-secreted cytokines from the same aptamer-functionalized electrode. *Biosens. Bioelectron.* **2015**, *64*, 43−50.
(44) Chen, Y.; Xu, L.-P.; Meng, J.; Deng, S.; Ma, L.; Zhang, S.; Zhang, X.; Wang, S. Superwettable microchips with improved spot homogeneity toward sensitive biosensing. *Biosens. Bioelectron.* **2018**, *102*, 418−424.

https://doi.org/10.1021/acsnano.2c00157
ACS Nano 2022, 16, 6266−6273